Phys Chem Minerals (1983) 9:95–101

PHYSICS AND CHEMISTRY OF MINERALS

Electron Paramagnetic Resonance and ENDOR Studies of $Cr^{3+}-Al^{3+}$ Pairs in Forsterite

L.V. Bershov[1], J.-M. Gaite[2], S.S. Hafner[3], and H. Rager[3]

[1] Academy of Sciences of the USSR, IGEM, Staromonetniy 35, 109017 Moscow, USSR
[2] Université d'Orléans, Laboratoire de Cristallographie, 45046 Orléans-Cedex, France
[3] University of Marburg, Institute of Mineralogy, Lahnberge, 3550 Marburg, West Germany

Abstract. The *electron paramagnetic resonance* (EPR) spectrum of Cr^{3+} in synthetic crystals of forsterite consists primarily of lines of Cr^{3+} "isolated" at the *M*1 and *M*2 positions in a "perfect" crystal environment without local charge compensation. In addition it shows two nonequivalent superhyperfine-split sextets with different intensities which are due to strong interaction of the Cr^{3+} electron spin **S** ($S=3/2$) with an adjacent nuclear spin **I**($I=5/2$). *Electron nuclear double resonance* (ENDOR) experiments revealed that the sextets result from $Cr^{3+}(M1)-Al^{3+}$ and $Cr^{3+}(M2)-Al^{3+}$ pairs, Al being located at adjacent tetrahedral Si sites. The **g**, **D**, **A**, and **A**′ tensor components of the $Cr^{3+}-Al^{3+}$ pairs have been determined at room temperature. The values of the pairs are distinct although they are not very different from the corresponding data of "isolated" Cr^{3+}. From the intensities of the EPR spectra the relative concentration of the $Cr^{3+}-Al^{3+}$ pairs with respect to "isolated" Cr^{3+} has been estimated.

Introduction

Electron paramagnetic resonance (EPR) allows the study of paramagnetic centers which may occur as more or less isolated defects in primarily diamagnetic crystals. Such centers may be produced e.g., by the substitution of small amounts of paramagnetic transition metal ions for diamagnetic ions at lattice positions. If the concentration of these centers is small and the crystal is otherwise of high perfection, an EPR spectrum with sharp lines may be expected. Under such conditions local details at the centers such as crystallographic point symmetry, site deformation, information on local chemical bonding etc. may be obtained with considerable accuracy. Natural forsterite Mg_2SiO_4 and magnesium-rich olivines $(Mg,Fe)_2SiO_4$ with $Fe/(Mg+Fe)$ ratios smaller than about 0.2 generally exhibit fairly sharp EPR spectra. However, they usually include a large number of different transition metal ions as minor or trace elements, e.g., Mn^{2+}, Ni^{2+}, Fe^{3+}, Cr^{3+} etc. so that complex EPR spectra are observed. Such spectra are difficult to interpret in view of the great many lines, even if the crystals are well analyzed chemically. Especially suitable for detailed EPR studies at the present stage are, therefore, well crystallized synthetic Mg_2SiO_4 crystals doped with certain paramagnetic impurities. Particularly straightforward are EPR studies of transition metal ions with half-integer electronic spins as e.g., Cr^{3+} in our case.

In the crystal structure of forsterite (space group *Pbnm*), transition metal ions generally substitute for Mg at the two distinct, octahedrally coordinated sites *M*1 (position 4*a*, point symmetry $\bar{1}$) and *M*2 (position 4*c*, point symmetry *m*). Less frequently, they may also substitute for Si at the tetrahedrally coordinated *Si* sites (position 4*c*, point symmetry *m*). The oxygen ions in forsterite have approximately hexagonal closed packing. Paramagnetic centers at octahedrally or tetrahedrally coordinated interstitial sites of that packing are expected to occur in very much smaller concentrations. Thus far, interstitial centers have not been identified in forsterite.

It is feasible to distinguish four general levels of splitting in the EPR spectrum of a paramagnetic center. If the spin states of a center with an effective spin $\mathbf{S}(S\geqq 1)$ are split due to the presence of a crystalline field the splitting is called *zero magnetic field* or *initial* splitting. Further splitting may be obtained by a superposed externally applied magnetic field which completely removes the residual spin degeneracy. The EPR lines which result from such a splitting are called *"fine" structure* (FS) lines. If the paramagnetic center also possesses a nuclear magnetic spin, **I**, the interaction of **I** with **S** yields additional *"hyperfine" structure* (HFS) of the FS levels. The HFS is characteristic for the paramagnetic center in question and reveals valuable, often unique information on the local chemical bonding, in addition to the crystallographic site information obtained from FS. So far, FS and HFS studies in forsterite have been carried out on $^{55}Mn^{2+}$ ($S=5/2$, $I=5/2$) (Gaite 1973), $^{57}Fe^{3+}$ ($S=5/2$, $I=1/2$) (Niebuhr 1976), and $^{53}Cr^{3+}$ ($S=3/2$, $I=3/2$) (Rager 1980).

Further perturbation of the spectrum in addition to FS and HFS may result from the interaction between **S** of the ion in question and the nuclear magnetic spin **I** of an adjacent atom, i.e., a ligand. This kind of interaction produces a ligand hyperfine or *"superhyperfine" structure* (SHFS) which, in general, provides direct crystallographic information on the local environment of the paramagnetic center. The adjacent atom may be either a regular atom of the crystal structure or a foreign atom which may substitute for a regular atom at a neighboring site and form an "impurity pair" together with the paramagnetic center. Interesting questions are identification of such a center-ligand pair and its particular chemical bonding in compari-

0342-1791/83/0009/0095/$01.40

son with the undisturbed crystal. In many cases, proper identification of the ligand may require *electron nuclear double resonance* (ENDOR) applied to the paramagnetic center and the nuclear spin of the ligand. Since ENDOR is a most sensitive method it provides a powerful means to locate crystal imperfections produced by impurity pairs in very small concentrations which generally cannot be studied by any other method.

A group of six weak but sharp, about equally spaced lines were detected some time ago (Rager 1978) in the EPR spectrum of synthetic forsterite doped with chromium, suggesting SHFS of an impurity pair. It has been the aim of subsequent work to identify and interpret this group of lines in cooperation between the Institute of Mineralogy, Marburg, and IGEM, Moscow. Some of the joint results have been published also in Russian (Bershov et al. 1981).

Experimental

EPR and ENDOR measurements were performed by use of two cubes with approximate dimensions of 3 and 7 mm, respectively, which were cut from two synthetic single crystal boules of forsterite doped with different amounts of Cr_2O_3. The boules were of cylindric shape with lengths of about 12 cm and diameters of 1.5 cm, grown by the Czochralsky method in the Crystal Synthesis Division of the Union Carbide Corporation. One fragment of each boule was analyzed by atomic absorption, which yielded 0.013 and 0.027 weight percent Cr. Assuming that Cr substitutes exclusively for Mg at the $M1$ and $M2$ positions and is distributed homogeneously over the boule, the respective formulas of the two crystals, no. 1 and no. 2, would be $(Mg_{0.9998}Cr_{0.0002})_2SiO_4$ and $(Mg_{0.9996}Cr_{0.0004})_2SiO_4$. It should be noted here that the distribution of Cr over the crystal is not expected to be perfectly homogeneous. However, the X-ray diffraction reflections in precession photographs were exceedingly sharp, indicating a regular crystallization with a highly perfect lattice. This was also confirmed by transmission electron microscopy (Godinou 1976) which revealed an unusually small density of about 2 linear dislocations per cm^2. The crystals studied by Godinou came from the same batch of forsterite boules grown by Union Carbide Coporation.

The EPR experiments were carried out at room temperature and X-band frequencies of 9.25, 9.49 and 9.52 GHz using 100 kHz modulation. A cylindrical cavity with a TE_{011} resonance mode was used. The angular dependence of the EPR spectra was determined by rotating the crystal around the crystallographic **a**, **b** and **c** axes. The rotation axis was perpendicular to the applied magnetic field **B**. B was varied between 0 and 1 T; it was calibrated by proton magnetic resonance. As notation for the coordinate systems, **a**, **b**, **c** is used for the crystallographic axes system, **X**, **Y**, **Z**, for the special crystal-bound system in the diagonalized matrix presentation, and **x**′, **y**′, **z**′ for the laboratory system, **z**′ being parallel to **B**.

The ENDOR experiments were performed at 6.48 MHz and 4.2 K at the Academy of Sciences of the Ukranian SSR, Kiev, USSR, using a home made superheterodyne type spectrometer. Experiment and interpretation of its results have been published recently in Russian (Bershov et al. 1981). In the following they are summarized briefly.

The resonance frequency in an ENDOR experiment is

$$\nu_{\mathrm{ENDOR}} = \left| \nu_n \pm \frac{1}{2} R \right| \tag{1}$$

where,

$$\nu_n = \frac{\gamma_I}{2\pi} \cdot B$$

is the *nuclear magnetic resonance* (NMR) frequency of the nucleus under consideration in the applied magnetic field **B**. γ_I is the nuclear gyromagnetic ratio of the spin **I**.

$$R = (A_{z'x'}^2 + A_{z'y'}^2 + A_{z'z'}^2)^{1/2}$$

is, in a first approximation, the frequency shift due to the hyperfine interaction **A** between the electronic field of the paramagnetic ion with effective spin **S** and the magnetic moment of the considered nucleus with spin **I** (Kevan and Kispert 1976). When the crystal is oriented so that the tensor is diagonal in the **x′y′z′** axis system, $R = A_{z'z'}$. R represents an effective hyperfine coupling for a particular orientation of the magnetic field with respect to the axes of the crystal. It will vary with orientation and include contributions of other components of the hyperfine tensor in general. From a complete study of the effective hyperfine interaction versus angle of rotation of **B** around three mutually perpendicular axes of a single crystal, all the components of the **A** tensor can be determined (Kevan and Kispert 1976). In this work the ENDOR experiment was performed by using Eq. (1) in order to obtain ν_n.

Results

The EPR spectra of both crystals comprize several groups of lines with stronger and weaker intensities. A spectrum of crystal no. 1 is shown in Fig. 1. Although the crystals were only doped with chromium sharp EPR lines due to very small amounts of Fe^{3+} and Mn^{2+} could also be identified in both samples. The strong, sharp lines in Fig. 1 (widths $<2\cdot10^{-4}$ T) are due to Cr^{3+} substituted for Mg^{2+} at the $M1$ and $M2$ positions (Rager 1977). They consist of typical "quintets": strong single FS lines of the Cr^{3+} isotopes which do not possess a nuclear spin ($I=0$) and

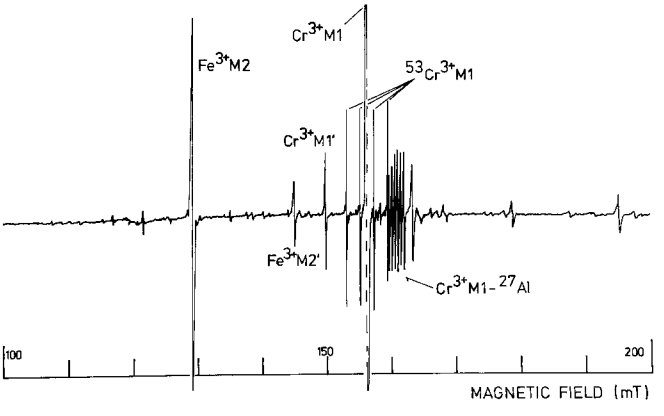

Fig. 1. EPR spectrum of a synthetic crystal of forsterite $(Mg_{0.9998}Cr_{0.0002})_2SiO_4$ at 9.524 GHz and 295 K. It shows FS single lines of Cr^{3+} at $M1$ and Fe^{3+} at $M2$ sites, an FS quartet of $^{53}Cr^{3+}$ (nuclear spin $I=3/2$) at $M1$ sites and an SHFS sextet of Cr^{3+} at $M1$ coupled with $^{27}Al^{3+}$ (nuclear spin $I=5/2$) at Si position. The crystal is oriented with **c**⊥**B** and **a** forms an angle of 45° with **B**

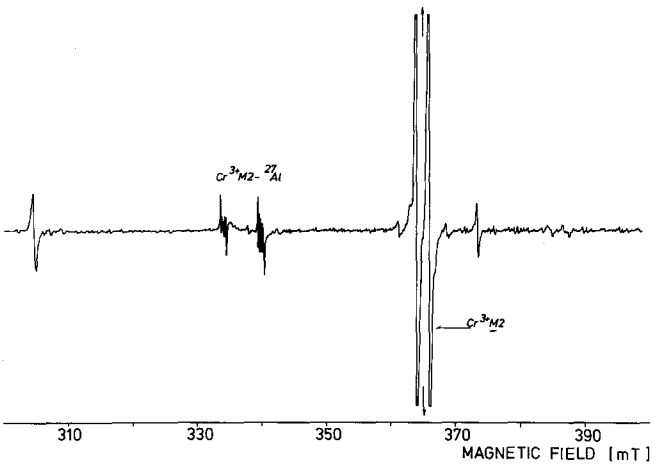

Fig. 2. EPR spectrum of forsterite $(Mg_{0,9996}Cr_{0,0004})_2SiO_4$ at 9.524 GHz and 295 K. It shows FS single lines of Cr^{3+} at $M2$ and SHFS sextet of Cr^{3+} at $M2$ coupled with $^{27}Al^{3+}$ at Si position. The crystal is oriented with $\mathbf{a} \approx \|\mathbf{B}$. The splitting is due to the angle of 2° between **a** and **B**. The sextet exhibits the correct point symmetry m for $M2$

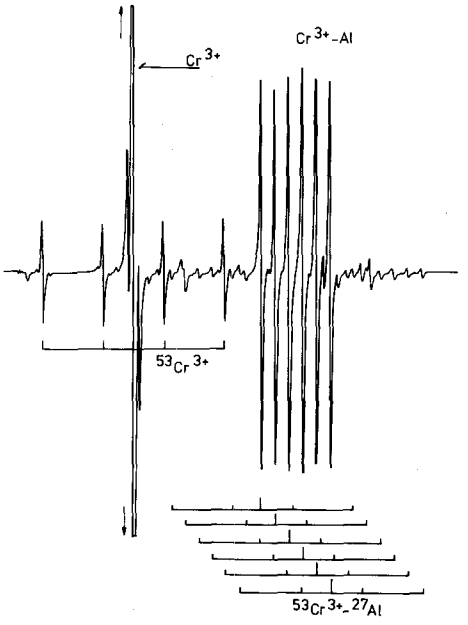

Fig. 3. EPR spectrum of forsterite (same crystal as Fig. 2) at 9.48 GHz and 295 K. It shows an FS line of Cr^{3+} in the center of the HFS quartet of $^{53}Cr^{3+}$ and an SHFS sextet of a $^{53}Cr^{3+}(M1)-{}^{27}Al$ pair center. Each of the six SHFS lines is the center of a weak $^{53}Cr^{3+}$ HFS quartet, thus providing the identity of Cr

HFS quartets of $^{53}Cr^{3+}$ ($I=3/2$) centered by the Cr^{3+} FS line. The smaller intensity of the quartet in comparison with the Cr^{3+} FS single line is in accord with the natural abundance of 10 percent of ^{53}Cr. Other less intense but sharp lines in Fig. 1 result from Fe^{3+} at $M2$. The observed Fe^{3+} centers in our crystals probably originate from very small contaminations of "chemically pure" MgO and silica gel used for crystal growth. The $Cr^{3+}(M2)$ and $Fe^{3+}(M2)$ lines of these two groups obey the point symmetry m of position $4c$. Other groups of lines include medium and weak signals which are not yet fully identified. Most of them are sharp. Some signals of these groups are definitely due to Cr^{3+}.

A fairly weak but unique group of lines are sextets which could be quite well resolved in both crystals. They were the primary focus of the present work. Two crystallographically nonequivalent sextets can be distinguished. Inspection of the particular splittings of the sextets depending on the crystallographic orientation with respect to **B** shows that the more intense set must be associated with Cr^{3+} at $M1$ (point symmetry $\bar{1}$) and the less intense one must be attributed to Cr^{3+} at $M2$ (point symmetry m; cf. Figs. 1 and 2). The identity of Cr^{3+} for these sextets is proved by the fact that each of the six lines has a quartet of weak satellites produced by $^{53}Cr^{3+}$ (cf. Fig. 3). The six lines are indicative of SHFS due to an interaction between Cr^{3+} and a nucleus with $I=5/2$ at a neighboring cation site. Moreover, from the fact that the sextets have no central lines it is concluded that this nucleus must belong to an isotope with 100 percent natural abundance. Therefore, ^{25}Mg ($I=5/2$) at an adjacent $M1$ or $M2$ site is excluded since the natural abundance of ^{25}Mg is 10.13 percent, the other Mg isotopes being spinless. Further, if the SHFS were due to ^{25}Mg the positional center of gravity of the sextet would coincide with that of the Cr^{3+} quintet. The observed SHFS sextet, however, is *significantly shifted.*

The dependence of the center of gravity position of the SHFS sextets on the orientation with respect to **B** was determined for both crystals by rotation around the crystallographic axes **a**, **b**, and **c**. The rotation around **a** for the more intense sextet is shown in Figure 4. The dependence

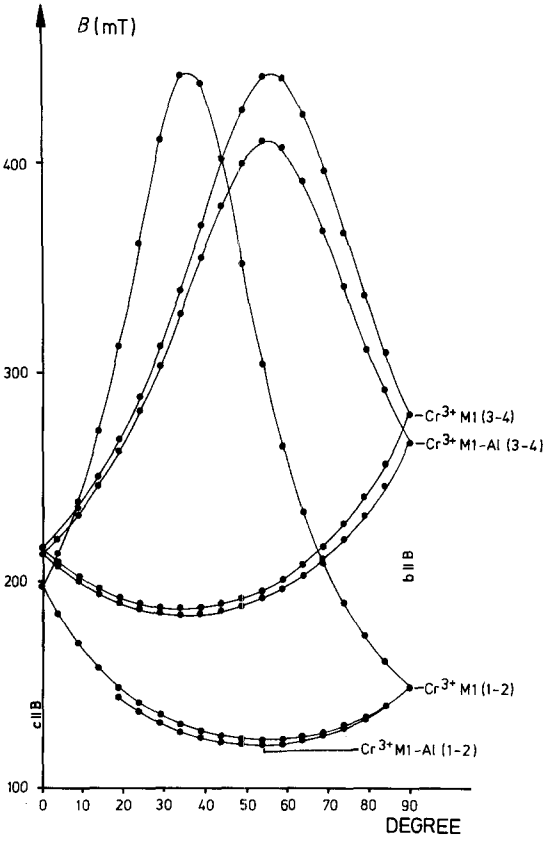

Fig. 4. Orientation dependence of the Cr^{3+} and Cr−Al pair EPR transitions at $M1$ in forsterite (**a** was the rotation axis). (1–2) and (3–4) denote the $3/2 \rightarrow 1/2$ and $-1/2 \rightarrow -3/2$ EPR transitions, respectively, for the Cr^{3+} electron spin $S=3/2$

exhibits considerable similarity with the Cr^{3+} ($M1$) FS lines. For evaluation of the center positions of the SHFS sextet, the Hamiltonian for FS transitions

$$\mathbf{H}=\beta(\mathbf{BgS})+\mathbf{SDS}$$
$$=\beta(g_Z S_Z B_Z+g_X S_X B_X+g_Y S_Y B_Y)+D_X S_X^2+D_Y S_Y^2+D_Z S_Z^2$$
$$=\beta(g_Z S_Z B_Z+g_X S_X B_X+g_Y S_Y B_Y)+D[S_Z^2-S(S-1)/3]+E(S_X^2-S_Y^2), \quad (2)$$

where $D=\frac{3}{2}D_Z$ and $E=\frac{1}{2}(D_X-D_Y)$ was used. Here, $\mathbf{S}(S=3/2)$ is the effective electron spin of Cr^{3+}; g_X, g_Y, g_Z and D_X, D_Y, D_Z are the principal components of **g** and **D** in the system **X, Y, Z** in which the FS tensor is diagonal, and β is the Bohr magneton. D (axial component) and E (rhombic component) are the conventional FS terms which describe the splitting of the Cr^{3+} ground state multiplet in the absence of an external magnetic field. Fitting the experimental data to the exact solution of the energy matrix of Eq. (2), the spin Hamiltonian parameters were obtained. They coincide for both crystals within the limit of error. The eigenvalues are listed in Table 1 and the eigenvectors in Table 2.

ENDOR signals were observed at all six SHFS lines. However, only the two central lines were considered because they were free from nuclear quadrupole contributions. The resulting experimental values of B and R [Eq. (1)] were $339.3\cdot10^{-4}$ T and $1.93\cdot10^{-4}$ T. For those nuclei which may be present in forsterite as additional impurities, like ^{55}Mn, ^{27}Al, $^{185+187}Re$, and ^{127}I, the frequencies ν_n and ν_{ENDOR} of Eq. [1] were calculated. They are listed in Table 3. Experimentally, the ENDOR frequency was found to be equal to $\nu_{ENDOR}=6.48\pm0.01$ MHz (Fig. 5). This is in agreement with ν_{ENDOR} of ^{27}Al. The sextet is, therefore, identified as resulting from a $Cr^{3+}-Al^{3+}$ pair center, designated in the following as (Cr−Al) center.

Including the hyperfine and superhyperfine interactions, Eq. (2) may be extended to

$$\mathbf{H}=(2)+\mathbf{IAS}+\mathbf{I'A'S'}.$$

Here **A** and **A'** denote the hyperfine interaction tensors between the electronic spin **S** and the magnetic moment **I** and **I'** of the respective ^{53}Cr and ^{27}Al nuclei. Using the perturbation method, the parameters A_X, A_Y, A_Z and A'_X, A'_Y, A'_Z of unpaired Cr^{3+} and the Cr−Al pairs at $M1$ and $M2$ were obtained in the system **X, Y, Z** (Bershov et al. 1981). The values are listed in Tables 1 and 2. Inspection of Table 2 shows that the principal axes **X, Y, Z** of the isolated Cr^{3+} centers and the Cr−Al centers are quite close to each other.

From the intensities **I** of the lines an estimate of the relative concentrations of the isolated Cr^{3+} centers and the Cr−Al pair centers is possible. The intensities of both centers depend primarily on the number N of the respective

Table 1. EPR data of isolated Cr^{3+} and Cr−Al pairs in forsterite[a]. The data are from two crystals $(Mg_{0.9998}Cr_{0.0002})_2SiO_4$ and $(Mg_{0.9996}Cr_{0.0004})_2SiO_4$. The SHFS was obtained from the crystal more enriched in chromium since the SHFS lines were more intense. The other crystal showed, however, a very similar spectrum yielding the same results

FS, HFS, and SHFS parameters	Cr^{3+} at position $M1$		Cr^{3+} at position $M2$	
	Isolated	Cr−Al	Isolated	Cr−Al
^{52}Cr FS data[a]				
g_x	1.980 (2)	1.981 (1)	1.970 (2)	1.978 (5)
g_y	1.980 (2)	1.978 (1)	1.979 (2)	1.981 (5)
g_z	1.974 (2)	1.975 (1)	1.970 (2)	1.975 (5)
D/GHz	30.6 (2)	23.6 (2)	21.1 (4)	25.8 (5)
E/GHz	8.48 (5)	5.28 (5)	2.60 (5)	0.30 (5)
$3E/D$	0.83	0.66	0.37	0.03
^{53}Cr HFS data				
A/MHz	46 (4)[b]	nd	50 (6)[b]	nd
A_x/MHz	51.8 (10)[c]	nd	nd	nd
A_y/MHz	48.3(10)[c]	nd	nd	nd
A_z/MHz	49.0 (10)[c]	nd	nd	nd
$^{52}Cr-^{27}Al$ SHFS				
A'_x/MHz	–	11.8 (3)	–	5.9 (5)
A'_y/MHz	–	8.6 (3)	–	4.5 (5)
A'_z/MHz	–	8.0 (3)	–	6.0 (5)

[a] cf. also Rager (1977); the data of this table are refined
[b] assumed to be isotropic; from Rager (1980a)
[c] this work
[d] the signs of the data were not determined experimentally. They have to be taken as absolute values

nd = observed, but not determined

Table 2. Directions of **D** of isolated Cr^{3+} and Cr−Al pairs in forsterite

Paramagnetic center	Principal directions of **D**[a]	Crystallographic axes (*Pbnm*)		
		a degree	**b** degree	**c** degree
Isolated Cr^{3+}				
$M1$	**X**	52.6	61.3	50.8
	Y	142.5	70.4	59.5
	Z	88.2	144.1	54.2
Cr−Al				
$M1$	**X**	51.5	60.1	52.4
	Y	141.7	69.6	59.0
	Z	87.4	142.7	52.8
Isolated Cr^{3+}				
$M2$	**X**	87.0	3.0	90
	Y	90	90	0
	Z	3.0	93.0	90
Cr−Al				
$M2$	**X**	82.7	7.3	90
	Y	90	90	0
	Z	7.3	97.3	90

[a] **X, Y, Z** is the system in which the FS term is diagonal

Table 3. Values of ν_n and ν_{ENDOR} for some isotopes having a nuclear spin $I=5/2$

Isotope	ν_n	ν_{ENDOR}
^{27}Al	3.766	6.47
^{55}Mn	3.583	6.28
^{127}J	2.906	5.61
^{185}Re	3.250	5.95
^{187}Re	3.284	5.98

ν_n is in MHz and calculated for $B_0=339.3\cdot10^{-4}$ T. ν_{ENDOR} is in MHz, the maximum error is ±0.07 MHz. The experimental ν_{ENDOR} frequency was 6.48 ± 0.01 MHz

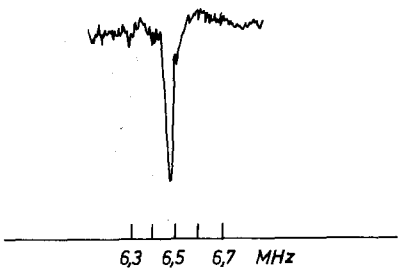

Fig. 5. ENDOR spectrum of ^{27}Al in forsterite at 4.2 K

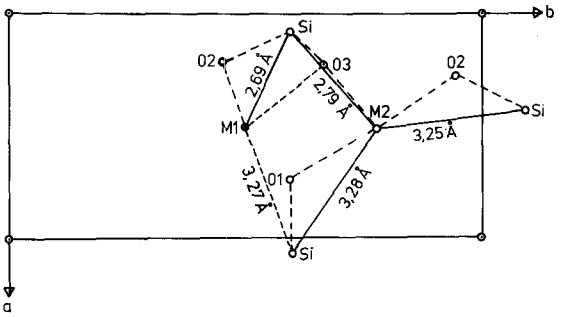

Fig. 6. Partial projection of the crystal structure of forsterite parallel **c** on the mirror plane. The space group is *Pbnm*

center in the investigated crystal. It should therefore be possible to estimate the proportion

$n = N_{Cr-Al}/N_{Cr^{3+}}$

In our case, the observed peak-to-peak widths, b, of the first derivatives of the lines were found to be approximately equal to or less than $2 \cdot 10^{-4}$ T. Because the linewidth depends also on transition and the orientation of the crystal with respect to **B**, we determined the intensities for the same orientation and transition. Using the relationship $I = b^2 \cdot h$ where h is the height of the signal we obtained at $M1$ for $(Mg_{0.9998}Cr_{0.0002})_2SiO_4$, $n = 0.12 \pm 0.05$, and for $(Mg_{0.9996}Cr_{0.0004})_2SiO_4$, $n = 0.25 \pm 0.05$. The n values seem to reflect the different Cr contents in the two forsterites. However, they should be proportional to the Al concentration. Therefore, the n values indicate the Al concentration to be smaller than the Cr concentration. This is in qualitative agreement with the investigation of the Cr and Al content in $(Mg_{0.9996}Cr_{0.0004})_2SiO_4$ using *secondary ion mass spectrometry* (Rager and Züchner, unpublished).

Discussion

Since Cr^{3+} is substituted for Mg^{2+} there is a nominal excess of positive charge, and the question of charge compensation is raised. The major fraction of Cr^{3+} which yields EPR lines with strong intensities is assumed to be at positions where any negative excess charge necessary for balance is *not* in the immediate Cr^{3+} environment which must be undisturbed over a certain range. This is supported by the very narrow line widths and the fact that the EPR spectrum of Cr^{3+} at $M2$ possesses the correct point symmetry m of that position. These paramagnetic centers are called "isolated". In contrast, the Cr–Al pair spectra require that the Al ions are very near the Cr^{3+} centers and are located at Si positions because of charge compensation. There is no information yet how charge balance of the isolated centers is achieved in the crystal structure. Since the concentration of Al^{3+} in our crystals is smaller than that of Cr^{3+}, substitution of Al^{3+} for Si^{4+} is not sufficient. Vacancies at Mg^{2+} positions which could be responsible for complementary balance were indeed reported by Pluschkell and Engell (1968). Some additional compensation might be expected to be due to proper electronic defects or interstitial ions. However, an EPR line at $g \approx 2$ with notable intensity could not be observed.

The Cr–Al Centers

The more intense sextets are assigned to Cr–Al centers, Cr^{3+} being located at an $M1$ site. There are two possible locations for Al as shown in Fig. 6: it may be located either at an adjacent tetrahedral Si site which shares a common edge with $M1$ ($d_{M1-Si} = 2.69$ Å) or at an adjacent Si site which shares a common apex with $M1$ ($d_{M1-Si} = 3.27$ Å). As the parameters $A'_i (i = X, Y, Z)$ at $M1$ (Table 1) are about ten times larger than e.g. those in $Cr:LaAlO_3$ (Taylor et al. 1973), it is concluded in view of this strong interaction that Al^{3+} must be located at the *nearest* Si site, which is edge-sharing with $M1$. Of course, the point symmetry of this center is then lowered from $\bar{1}$ to 1 by Al substitution for Si. From Table 2 it is seen that the eigenvectors **X**, **Y**, **Z** of the Cr($M1$)–Al center do not deviate substantially from the ones of the isolated Cr^{3+} ($M1$) center.

In the following, a simple geometrical model is considered on a qualitative basis. The Cr–Al **X** axis is found to be fairly parallel to the direction from $M1$ to the nearest Si position. $A'_X = 11.8$ MHz (cf. Table 2) is the largest value of **A'** whereas A'_Y and A'_Z are smaller and almost equal. Thus in a first approximation, **A'** may be separated into an isotropic and anisotropic contribution, A'_i and A'_a respectively, according to

$$A' = A'_i + A_a(3\cos^2\theta - 1) \quad (3)$$

A'_i arises from the presence of unpaired s electrons at Al^{3+} and A'_a from unpaired p_σ and p_π electrons together with the dipolar interaction A'_{dd} between the ^{27}Al nucleus and the effective Cr^{3+} electronic spin. θ is the angle between **B** and the Cr–Al direction. Extremum values of A' occur for $\theta = 0$ and $\theta = 90°$. The A' data of Table 2 combined with Eq. (3) yield $A'_i = 9.4$ MHz and $A'_a = 1.15$ MHz. A'_{dd} can be calculated from the relationship

$$A'_{dd} = \mathbf{g}_n\beta_n\mathbf{g}\beta/r^3 \quad (4)$$

where $\mathbf{g}_n\beta_n$ is the ^{27}Al nuclear magnetic moment, $\mathbf{g}\beta$ the Cr^{3+} magnetic moment, and $r = 2.69$ Å the distance between $M1$ and the nearest Si site. Equation (4) yields $A'_{dd} = 1.05$ MHz, which is nearly the experimental value $A_a = 1.15$ MHz. This indicates that the net contribution of the unpaired p_σ and p_π electrons is small. Thus, A_a is dominated by a dipole-dipole interaction and hence supports our conclusion that Cr^{3+} at $M1$ interacts with Al^{3+} at the nearest Si site.

The line intensities of the Cr($M2$)–Al center is substantially lower and its relative resolution is less than for the Cr($M1$)–Al center (cf. Figs. 1 and 2). For this reason, the **A'** data for $M2$ are less precise. Considering their rather large errors, a decomposition of **A'** into an isotropic and anisotropic term does not appear feasible. The fairly great values of **A'** are, however, consistent with a short distance

between the two coupled spins. Inspection of the EPR spectrum shows that the symmetry of the Cr($M2$)−Al center remains m. Therefore, both ions of the Cr−Al center must be located in the mirror plane. For an $M2$ site, there are three neighboring Si tetrahedra within the mirror plane, one Si site sharing a common edge ($d_{M2-Si}=2.79$ Å) and two Si sites sharing a common apex ($d_{M2-Si}=3.25$ Å, 3.28 Å). This is illustrated in Fig. 6. As only one Cr($M2$)−Al sextet is observed, Cr^{3+} at $M2$ interacts with Al^{3+} at one distinct site; otherwise more than six SHFS lines ought to be observed (Zwingel 1976; Schirmer et al. 1975). Thus, the question arises which of the three Si positions around a Cr^{3+}($M2$) center is most probably occupied by Al^{3+}.

The Coulomb attraction alone favors the Cr^{3+}($M2$)−Al^{3+}(Si) pairs with the shortest distance $r=2.79$ Å. Then a more anisotropic contribution to **A**′ could be expected, as has been found for the Cr^{3+}($M1$)−Al^{3+}(Si) pairs ($r=$ 2.69 Å). However, this is not the case and we will consider the possibility that for the Cr^{3+}($M2$)−Al^{3+}(Si) pairs Al is located at the next nearest Si position. Thus,we are left with the two Si tetrahedra sharing a common apex with the $M2$ oxygen octahedron.

Because the spin transfer from Cr^{3+}($M2$) to Al^{3+}(Si) can occur via the oxygens $O2$ or $O1$ (Fig. 6), the junction lines $M2-O2-$Si and $M2-O1-$Si will be considered in more detail. The $M2-O2-$Si path contrasts with the $M2-O1-$Si one in their respective bond lengths. The $M2-O2$ distance ($r=2.05$ Å) is smaller than the $M1-O1$ one ($r=2.182$ Å) whereas the $O2-$Si distance ($r=1.65$ Å) is larger than the $O1-$Si one ($r=1.61$Å). Thus, the apparent covalent participation of $O2$ with a cation at $M2$ should be expected to be larger than that of $O1$. This may also be confirmed by the fact that the **Z** eigenvectors of the Fe^{3+}($M2$) and Mn^{2+}($M2$) **g** tensors are nearly parallel to the $M2-O2$ direction (Rager 1980b).

Although this correspondence was not observed for Cr^{3+} (Rager 1980b) the coupled, charge compensated substitution

$$Mg^{2+}(M2)+Si^{4+}(Si)=Cr^{3+}(M2)+Al^{3+}(Si)$$

may also be affected by the distances and the bonding situation on the $M2-O2-$Si path, i.e., the spin transfer from Cr^{3+}($M2$) to Al^{3+}(Si) probably runs through $O2$. Thus, based on chemical arguments and the fact that only one Cr($M2$)−Al center was observed the Si position which is 3.25 Å apart from $M2$ may preferentially be occupied by Al ions.

However, it should be emphasized that this is only an attempt to answer the question which of the three possible Si positions around Cr^{3+}($M2$) is occupied by Al^{3+}. Finally, we want to mention that the considerable difference between the SFHS data at $M1$ and $M2$ (Table 1) cannot be explained at the moment. Only this should be noted: the smaller superhyperfine interaction in the Cr^{3+}($M2$)−Al^{3+}(Si) pair corresponds to the larger ionic bonding character of Cr^{3+} at $M2$ (Table 1, Rager 1980a).

Local Symmetry of the Cr−Al Centers

In view of the small concentrations of Cr^{3+} in our crystals and the small proportion of Cr^{3+} interacting with Al, the Cr−Al centers are assumed to be entirely isolated in Mg_2SiO_4. Such paramagnetic pair centers may exhibit a primarily axial symmetric crystal field (Kirkpatrick et al. 1964) which can be examined from $3E/D$ ratios (Table 1). $3E/D$ represents the deviation of the crystal field tensor from axial symmetry and is a measure of the asymmetry of the local crystal field. It may be compared also with $\eta=(V_{XX}-V_{YY})/V_{ZZ}$ of the nonsubstituted Mg^{2+} positions which were determined using NMR (Derighetti et al. 1978). Here, V_{XX}, V_{YY}, and V_{ZZ} are the second derivatives of the electrostatic potential at ^{25}Mg sites.

At $M2$ $\eta(Mg^{2+})=0.39$, $3E/D$ (Cr^{3+} isolated)$=0.36$, and $3E/D$ (Cr−Al)≈ 0. The local symmetry at $M2$ has often been approximated by $3m$ symmetry (Burns 1970) with the pseudo-trigonal axis along the crystal **a** axis. Although **Z** of Cr^{3+}($M2$) isolated is approximately parallel to **a** (Table 2) the $3m$ symmetry does not apply for isolated Cr^{3+} ($M2$) centers as pointed out by Rager and Weiser (1981). Moreover, **Z** of the ^{25}Mg quadrupole tensor makes an angle of 18° with **a**. Thus, irrespective of the occupation of $M2$ by an impurity or by a structural atom the local symmetry cannot be described by $3m$. In the case of the Cr($M2$)−Al center $3E/D\approx 0$ indicates a local axial symmetry which is assumed to be due to the nearby charge compensating Al^{3+} ion. The effect of nearby charge compensators on the size of D and E and also on the orientation of **Z** is well known. However, in a detailed discussion atomic shifts due to coulomb attraction and lattice relaxation effects have to be considered.

Further it remains to be investigated whether the influence of the charge compensator is a direct one or runs through the ligands. Therefore, our attempts to explain the difference in size and orientation between the two FS terms of isolated Cr^{3+} and Cr−Al considering the superposition model of Newman and Urban (1975) were not successful.

At $M1$ η (Mg^{2+})$=0.96$, $3E/D$(Cr^{3+} isolated)$=0.83$, and $3E/D$(Cr−Al) ≈ 0.6. Although the asymmetry parameter of the Cr($M1$)−Al centers appears to be slightly reduced by the adjacent single Al^{3+} ion, in general the asymmetry of the local crystal field at $M1$ remains high. This is in contrast to what one would expect taking the above discussed Cr($M1$)−Al and Cr($M2$)−Al distances into account. However, electric field gradient calculations on the basis of an extended point ion model (Rager and Schmidt 1981) also yielded a high asymmetry parameter η at $M1$ in qualitative agreement with the above data. This suggests that the topology of the crystal structure of forsterite, i.e., the extended environment of the $M1$ position, mainly determines the high asymmetry of the crystal field at $M1$.

Acknowledgement. This work was supported by the German Research Foundation (Grant SFB-127).

References

Bershov LV, Mineeva RM, Speransky AV, Hafner SS (1981) The entry of chromium and aluminium into the forsterite structure based on electron paramagnetic resonance (EPR) and double electron nuclear resonance (DENR) data. Mineral. Zhurnal 3:662–70 (in Russian)

Burns RG (1970) Mineralogical applications of crystal field theory. Cambridge University Press, Cambridge

Derighetti B, Hafner SS, Marxer H, Rager H (1978) NMR of ^{29}Si and ^{25}Mg in Mg_2SiO_4 with dynamic nuclear polarization technique. Phys Lett A 66:150–151

Gaite J-M (1973) Etude de propriétés locales dans les cristaux

de basse symétrie à l'aide de la résonance paramagnétique electronique d'ions à l'etat S, Dissertation, Université d'Orleans
Godinou D (1976) Déformation plastique a haute température de monocristaux de forsterite. Dissertation 3me cycle. Université Claude Bernard Lyon 1
Kevan L, Kispert LD (1976) Electron spin double resonance spectroscopy. John Wiley and Sons, New York
Kirkpatrick ES, Müller KA, Rubins RS (1964) Strong axial electron paramagnetic resonance spectrum of Fe^{3+} in $SrTiO_3$ due to nearest neighbor charge compensation. Phys Rev A 135:86–90
Newman DJ, Urban W (1975) Interpretation of S-state ion EPR spectra. Adv Phys 24:793–844
Niebuhr H (1976) Elektronen-Spin-Resonanz von dreiwertigem Eisen in Forsterit. Habilitationsschrift, FB Geowissenschaften, Marburg
Pluschkell W, Engell HJ (1968) Ionen- und Elektronenleitung in Magnesiumorthosilikat. Ber Dtsch Keram Ges 45:388–394
Rager H (1977) Electron spin resonance of trivalent chromium in forsterite Mg_2SiO_4. Phys Chem Minerals 1:371–378
Rager H (1978) New spectroscopic results of Fe^{3+} and Cr^{3+} in Mg_2SiO_4. Phys Chem Minerals 3:88–89
Rager H (1980a) Electron-nuclear hyperfine interactions of $^{53}Cr^{3+}$ in Mg_2SiO_4 (forsterite). Z Naturforsch Teil A 35:1296–1303
Rager H (1980b) Electric field gradients and asymmetry parameters of Fe^{3+}, Mn^{2+}, Cr^{3+} and Mg^{2+} in Mg_2SiO_4. J Mol Struc 58:215–220
Rager H, Schmidt PC (1981) Electric field gradient calculation in forsterite, Mg_2SiO_4. Phys Chem Minerals 7:169–176
Rager H, Weiser G (1981) Polarized absorption spectra of trivalent chromium in forsterite, Mg_2SiO_4. Bull Minéral 104:603–609
Schirmer OF, Blazey KW, Berlinger W (1975) ESR and optical absorption of bound, small polaron on $YA1O_3$. Phys Rev B 11:4201–4211
Taylor DR, Owen J, Wankley BM (1973) Hyperfine interactions and electron transfer between metal ions in $Fe:LaAlO_3$ and $Cr:LaAlO_3$. J Phys C 6:2592–2610
Zwingel D (1976) The structure of trapped hole centers in Al-doped TiO_2. Solid State Commun 20:397–400

Received March 11, 1982